Heterointerface Engineering of Cerium Fluoride Confined Molybdenum Nitride for Overall Water Splitting

Arokiadoss Davidrichetson, ‡Sundararajan Arivudainambi, Mayakrishnan Raj kumar, Murugan Vijayarangan, Jayaraman Jayabharathi*

Department of Chemistry, Materials Science Lab, Annamalai University, Annamalai nagar, Chidambaram, Tamilnadu 608002, India

‡Department of Entomology, Faculty of Agriculture, Annamali University, Annamalinagar, Chidambaram and Tamil Nadu

*Corresponding author-. *jjayabharathi2022@gmail.com*

This file contains 28 pages in which the experimental section consists of materials and methods, characterization of an electrocatalyst, electrode preparation and characterization and Faradaic efficiency determination from RRDE.

No. of Figures- 14; No. of Equations- 13; Tables- 5

SI-I. Experimental Section

S1-E1. Materials

$(NH_4)_6Mo_7O_{24}\cdot 4H_2O$, NH_4F and $Ce(NO_3)_3\cdot 6H_2O$ was received from SISCO CHEM. Nickel Foam (NF) received from Vitra Technologies, India. Iridium oxide (IrO_2), platinum derived carbon (Pt-C), Nafion 15% and alumina mesh received from Sigma Aldrich. All chemicals used as received without any further purification. The Deionized water was used throughout the experiment.

S1-E2. Characterization of an electrocatalyst

High resolution transmission electron microscopy (HR-TEM) conducted on a JEOL JEM 2200FS microscope operated at 200 kV acceleration voltage, probe-side C_s-corrected, integrated with an Oxford X Max 100 Energy Dispersive X-ray (EDX) detector. Field Emission Scanning Electron Microscopy (FE-SEM) was conducted on ZEISS oxford and an accelerated voltage at 3 kV with the measurement of EDX. Structural interpretation of CoO_x-Bo identified with x-ray diffraction (XRD), were taken on a powder diffractrometer (Rigaku, D/MAX, 2500 V) with Cu Kα radiation (λ=1.54056 Å) operating at 40 KV and 250 mA. Chemical bond structure identified based on Fourier Transform Infrared (FT-IR) spectrometer Thermo Nicolet 6700. Raman measurement was carried out at room temperature, and the signals were recorded by using Raman spectroscopy (Renishaw) with a 514.5 nm laser excitation. XPS measurements were carried out in an ultra-high vacuum (UHV) set-up equipped with a monochromatic Al Kα X-ray source (1486.6 eV; anode operating at 12.25 kV and 300 W) and a high resolution Phoibos 150 MCD analyzer (SPECS). X-ray photoemission spectra were measured in fixed analyzer transmission mode with pass energy 20 eV and step size 0.5 and 0.05 eV for survey and region scans correspondingly.

S1-E3. Electrode preparation and characterization

All electrochemical measurements were carried out on a Biologic SP-300 Potentiostat electrochemical workstation, the linear sweep voltammogram (LSV) test was carried out in 1 M KOH electrolyte with a scan rate of 10 mV/s three-electrode setup. To prepare catalyst ink, 0.5 mg of the as-prepared CeF_3@Mo_2N was evenly dispersed in 0.5 mL of propanol, and then the as-obtained solution was treated with ultrasound for 20 min. For comparison, a 0.005 mg/ml commercial IrO_2 and Pt/C suspension was made using a comparable methodology. Before coating, the NF was washed with acetone, HCl aqueous solution, deionized water and ethanol in sequence. In a three-electrode setup nickel foam (NF) as the working electrode, Ag/AgCl (3M KCl) as reference electrode, and a platinum wire as counter electrode. Measured potentials were referred to the reversible hydrogen electrode (RHE) $E_{RHE} = E_{Ag/AgCl} + 0.923$ V. The resistances of as prepared electrocatalysts were acquired from EIS tests at the overpotential of different mV (vs. RHE) in the frequency scope of 100 kHz to 10 mHz. The durability was tested by cyclic voltammetry (CV) and current-time (i-t) curve tests.

SI-E4. Faradaic efficiency determination from RRDE

In order to evaluate the faradaic efficiency and reaction mechanism of CeF_3@Mo_2N catalyst for OER, rotating ring-disk electrode (RRDE) voltammograms were carried out based on a glassy carbon disk electrode and Pt ring electrode. The CeF_3@Mo_2N catalyst, as prepared, was coated onto RRDE by following the procedure described above. The Faradaic Efficiency for CeF_3@Mo_2N in OER process was calculated by using Rotating

Ring-Disk (RRD) technique as follows:

Ring current (I_{ring}) = 0.0379 mA

Disc current (I_{disc}) = 0.1750 mA

Collection Efficiency (N) = 0.235 (The Collection Efficiency (N) value calculated experimentally by using ferri/ferrocyanide system in 0.1 M KCl with 10 mM $K_3[Fe(CN)_6]$, the data are given Table

SI-II. Calculations

SI. C1. Calculation of Overpotential (η)

The overpotential (η) was determined according to the formula: η (V) = E (RHE) - 1.23 V

SI. C2. Calculation of Tafel slope

Tafel plots were derived from the LSV curves and the Tafel slope was calculated using the equation: η = a + b log j, where η-overpotential, a-exchange current density, b -Tafel slope and j- corresponding current density (mA /cm^2) as well as Tafel constant

SI. C3. Calculation of ECSA

The calculations of ECSA and roughness factor (RF) are based on the following equation: ECSA= C_{dl} /C_s; RF=ECSA/GSA, where C_{dl}- double layer capacitance of catalyst in 1.0 M KOH (mF) and C_s- specific capacitance of the catalyst (C_s = 0.04 mF cm^{-2} in 1.0 M KOH). In eq (5), RF - roughness factor and GSA - geometric surface area of the material.

SI.C4. Calculation of Specific Activity

The specific activity (mA/cm^2 $_{ECSA}$) of electrocatalysts was calculated by the equation of:

(i) Specific activity = j/10 x $ECSA_{BET}$ x amount of loading

(ii) Specific activity = j/10 x $ECSA_{Cdl}$ x amount of loading

SI.C5. Calculation of Turnover frequency (TOF), Active site density and Nature of the charge storage process

The TOF is defined as the number of H_2 or O_2 molecules evolved per active site per second.

TOF of O_2 or H_2 = $TOF = i\frac{S_{geo}}{4Fm}$, where, where j, S_{geo}, F, and m signified current density (mA/cm^2), geometric surface area (cm^2) of the working electrode, Faraday constant (96,485 C/mol) and moles of the active catalyst species, respectively. For TOF analysis, determination

of concentration (m) of surface active species is a major challenge. Finding the position of active centers can provide the necessary guidance to determine m. To know the active site concentration, i versus $v^{1/2}$ was plotted using the following equation

$$i = \pm 0.436nFA_{real}\, C\sqrt{nF\, Dv/RT}$$

The number of active sites is attributed by ($A_{real}C$), where A_{real} and C refer to total electrochemical area and active site concentration, respectively. The C, D, and A_{real} manifest the per-site concentration, diffusion constant and electrochemical area, respectively. The active site density was calculated by considering D = 1 and n = 1.Identifying the position of the catalytically active centers in the catalyst by using the following mathematical expression can provide the necessary guidance to accurately determine m$i = a\upsilon^{b}$; $\log i = \log a + b\log \upsilon$, b value was calculated from the log(current) versus log(scan rate) plot, where i and ν denote the current and scan rate, respectively. For b ~ 0.5, the ion intercalation (diffusion) mechanism predominates, indicating that majority of the active sites are at the interlayer spacing, while a surface-controlled process is expected for b ~ 1.

SI. C6. Faradaic efficiency determined from RRDE

In order to evaluate the faradaic efficiency and reaction mechanism of CeF_3@Mo_2N catalyst for OER, rotating ring-disk electrode (RRDE) voltammograms were carried out based on a glassy carbon disk electrode and Pt ring electrode. The CeF_3@Mo_2N catalyst, as prepared, was coated onto RRDE by following the procedure described above. The Faradaic Efficiency for CeF_3@Mo_2N in OER process was calculated by using Rotating

Ring-Disk (RRD) technique as follows:

Ring current (I_{ring}) = 0.0379 mA

Disc current (I_{disc}) = 0.1750 mA

Collection Efficiency (N) = 0.235 (The Collection Efficiency (N) value calculated experimentally by using ferri/ferrocyanide system in 0.1 M KCl with 10 mM $K_3[Fe(CN)_6]$, the data are given in Table.

SI. C7. Determination of energy of activation

With the CVs results, we can obtain the apparent activation energy (E_a) calculated using the Arrhenius equation: ln j = -Ea/RT +b, where j- current density, R-gas constant, T-Temperature and b-slope.

SI. C8. Calculation of rate constant

The rate constant of the electrolysis at various pH was determined from Trumpet plot by following $k_0 = (1-\alpha)nFv_a/RT$, where R-gas constant, T-absolute temperature, α-electron transfer coefficient, n-number of electrons transferred and v_a and v_c are anodic and cathodic slopes of the Trumpet plot, respectively.

SI. C9. Calculation of Laviron equation

$Ec = E_{1/2} – (RT/\alpha nF) \times \{\ln(\alpha nF/RTks) + \ln(\upsilon)\}$, where Ec is the reduction potential of metal redox, E1/2 is the formal potential of metal redox, R is universal gas constant, T is temperature in Kelvin, n is number of electrons transferred, F is the Faraday constant, α is the transfer coefficient, ks is the rate constant of metal redox, and υ is scan rate in the CV measurement. The Laviron analysis highlights the peak positions of redox peaks prior to OER at different scan rates in materials, while other parameters including R, T and n are taken from literatures. ks and α values can be concluded from the intercept and slope of the linear plot of Ec with respect to ln υ. Herein, the rate constant of metal redox ks derived from equation can be used to qualitatively compare the binding strength of Ni sites to OH- in electrolyte. The larger ks, the enhanced OH adsorption.

SI. C10. Proton reaction order (ρRHE)

The proton reaction order (ρRHE) was determined on RHE scale from the following relation

$$\rho_{RHE} = \left(\frac{\partial log\,(i)}{\partial pH}\right)_E = -\left(\frac{\partial E}{\partial pH}\right)_i / \left(\frac{\partial E}{\partial\, log(i)}\right)_{pH}$$

SI. C11. Calculation of H_2 and O_2 generation

Based on the displaced amount of water due to the hydrogen bubbles the amount of hydrogen generated was calculated using the below relationships.

Amount of O_2 generated in 1 h = Amount of water displaced in litres

Amount of O_2generated in moles for 1 h = $\frac{\text{Amount of water displaced (liters)}}{22.4 \text{ liters}}$

The O_2 generation rate was calculated from the electrical charge passed through the electrode using the equation given below.

Current obtained during electrolysis x Time duration for each potential = Coulomb

$\frac{\text{Coulomb x F}}{96485C}$ = No. of moles of e^- for H_2/O_2 generation

$\frac{\text{No. of moles of } e^- \text{ for } H_2 \text{ or } O_2 \text{ generation x 1 mole of } H_2 \text{ or } O_2 \text{ gas}}{4/\ 2 \text{ moles of electron generated}}$ = Moles of H_2/O_2

SI. C12. Faradaic efficiency

At the constant potential of 1.59V given across the CeF_3@Mo_2N/NF//CeF_3@Mo_2N/NF electrode couples assembled and sealed in H-type full cell in 1.0 M KOH. During the electrolysis, evolved gas molecules were measured by the water displacement method. The applied potential can provide 10 mA cm^{-2} current density to the system and the electrolysis was monitored for 60 min. each 10 minutes of analysis data shown in the data. Theoretical number of moles of gas molecules can be calculated from Faraday's second law of electrolysis according to the following equation: Vt=Q/nF, where Vt - number of O_2 molecules calculated theoretically, Q-total charge passed to the cell systems, n-number of electrons (n=4 for O_2) and

F-Faraday constant 96485.3 C/mol. The Faradaic Efficiency of OER was estimated using the following equation: $FE = 4Fn_{O2}/It \times 100\%$, where F is Faraday constant (96485 C/mol), n_{O2} is the number of moles of experimental O_2 during the reaction (mol), n_{H2} is the number of moles of experimental H_2 during the reaction (mol), I is the current of the reaction (A), and t is the reaction time (s).

SI. C13. Determination of Power consumption

Based on Faraday's law, power consumption for water electrolysis process can be expressed as follows: Energy consumption ($kWhm^{-3}$) = V_{cell} x nF/3600 x1/$V_{m,}$ where, V_{cell} - voltage during electrolysis, n - number of electrons (4 for OER: 2 for HER), F -Faraday constant of 96,500 C mol^{-1} and V_m - molar volume of gas to be 24.47 L mol^{-1} at 25 °C and 1 atm.

SI-III. Figures

Figure S1. Elemental mapping of CeF_3@Mo_2N: (a) Ce; (b) Mo; (c) F; (d) N and (e) EDX spectrum of CeF_3@Mo_2N

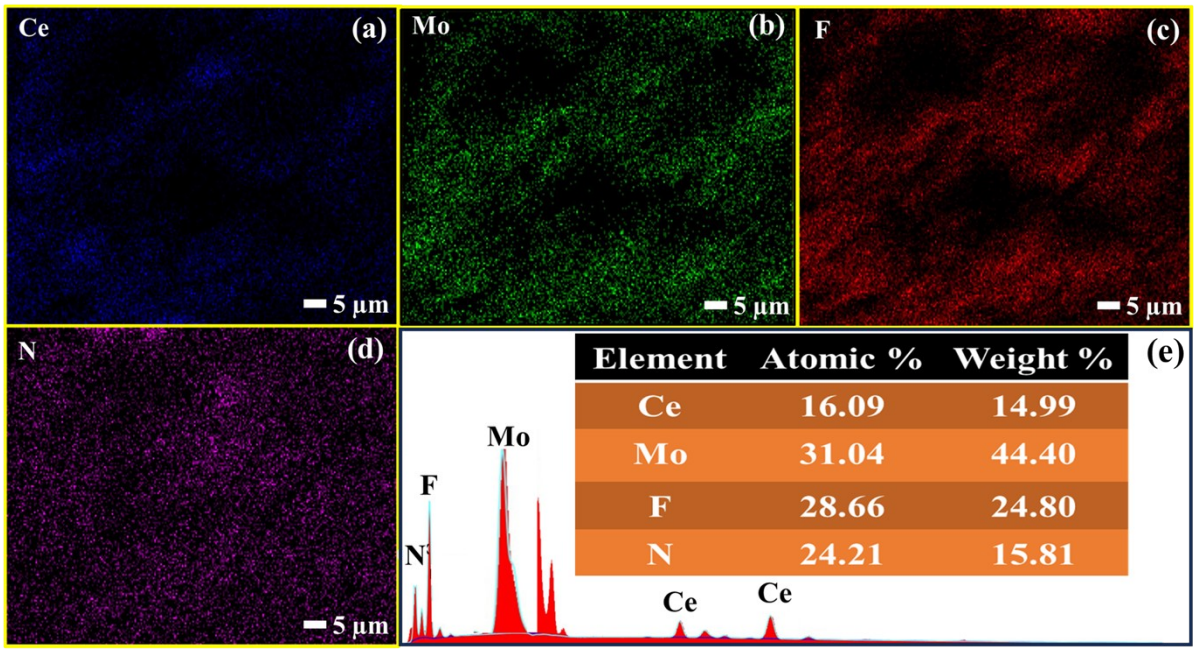

Figure S2. Static water contact-angle measurements with illustration of O_2 bubbles releasing behaviour of the electrodes

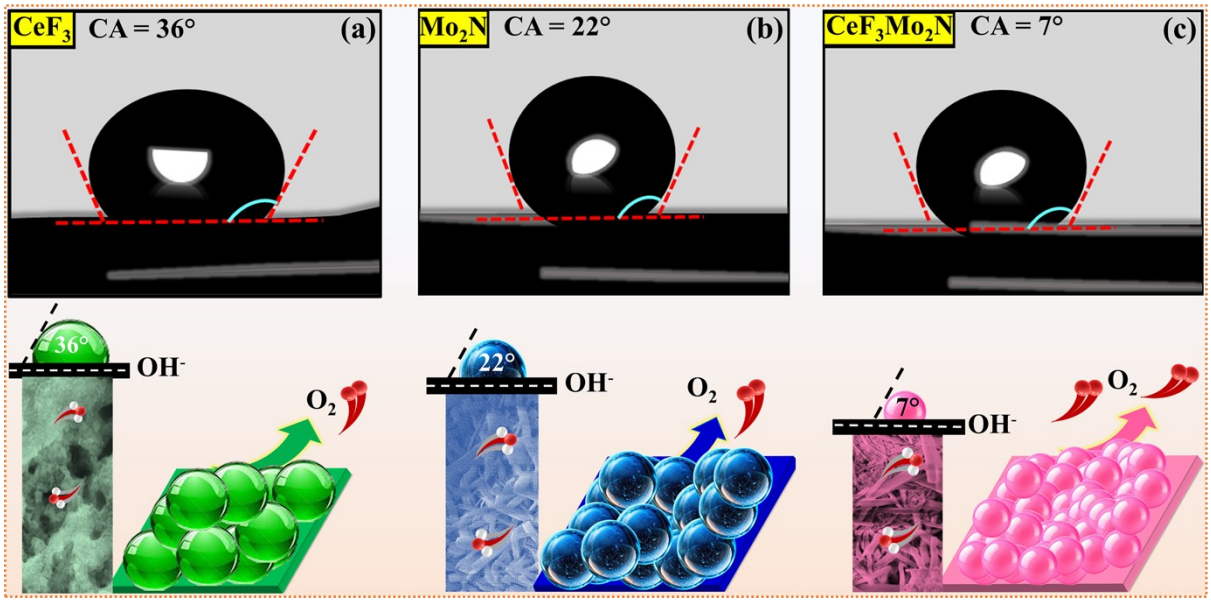

Figure S3. CVs recorded at non-faradaic region to estimate the Cdl values: (a) CeF_3@Mo_2N; (b) Mo_2N and (c) CeF_3

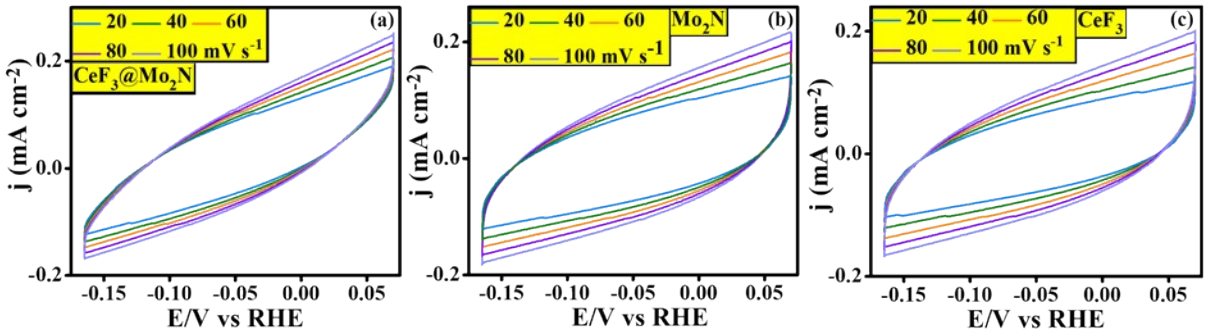

Figure S4. (a) ECSA-Normalized LSV curves, (b) Bet-Normalized LSV curves (c) Mass Normalized LSV curves (d) Mass activity of as prepared electrocatalysts, (e) Plot of logi vs logυ to determine catalytic site density and (f) TOF-Normalized LSV curves of OER

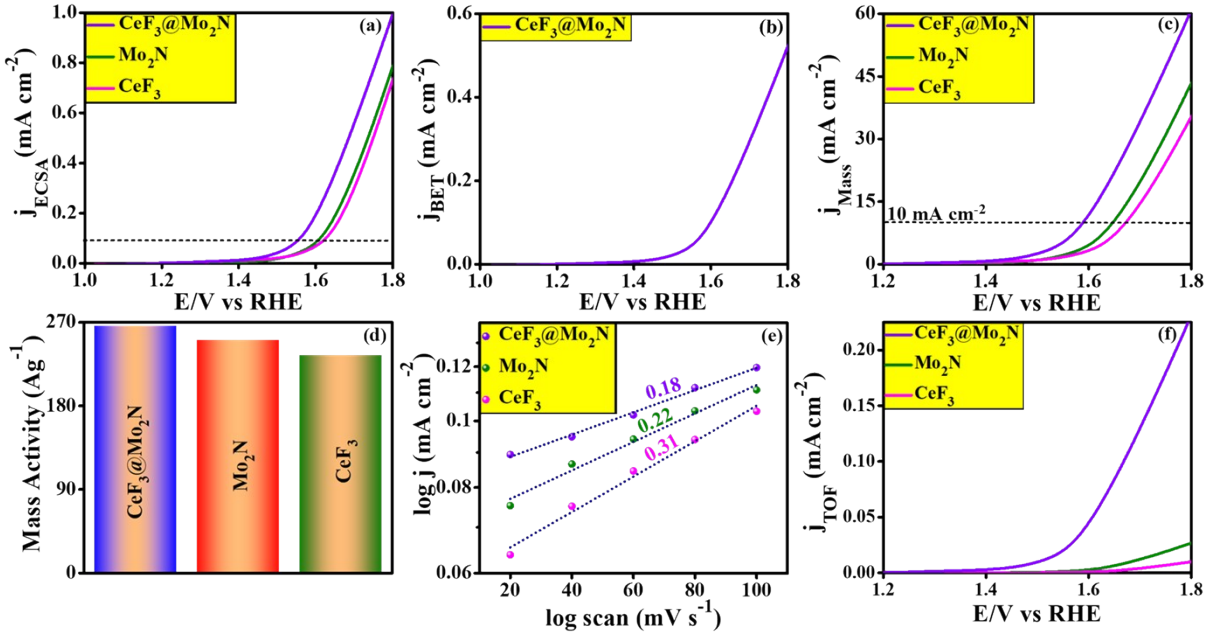

Figure S5. (a) LSV responses of RRD electrode for redox reaction of ferro-ferric in 0.1 M KNO_3 with 10 mM of $K_3[Fe(CN)_6]$ at various rotation speed by using RRD electrode, (b) Equivalent circuit model used to analyse interfacial electron transfer and (c) Operando dynamic specific resistance at OER overpotential of CeF_3@Mo_2N, Mo_2N and CeF_3 in 1M KOH

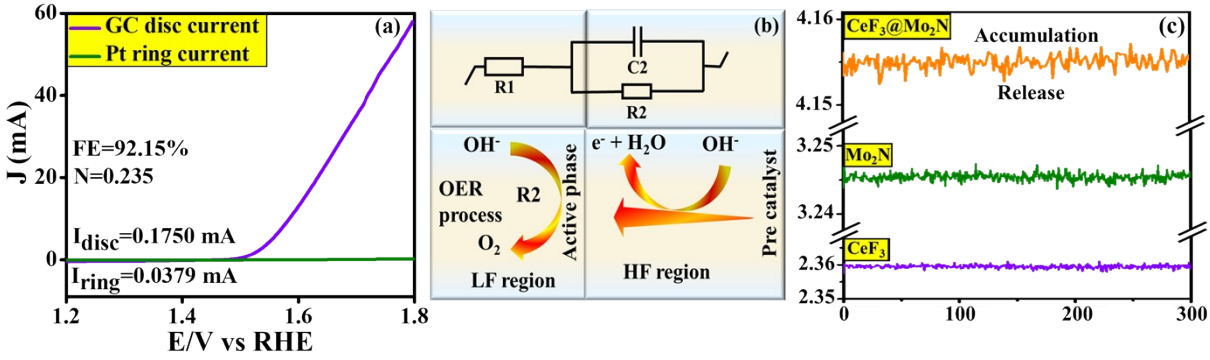

Figure S6. Cyclic voltammogram of CeF_3@Mo_2N at various pH: pH-14 (a), pH-13 (b) and pH-12 (c) with potential range of 10-100 mV and peak potential of CeF_3@Mo_2N with respect to logarithm of scan rate [V/s] during CV at pH-14 (d), pH-13 (e) and pH-12 (f) (violet: anodic peak; green: cathodic peak)

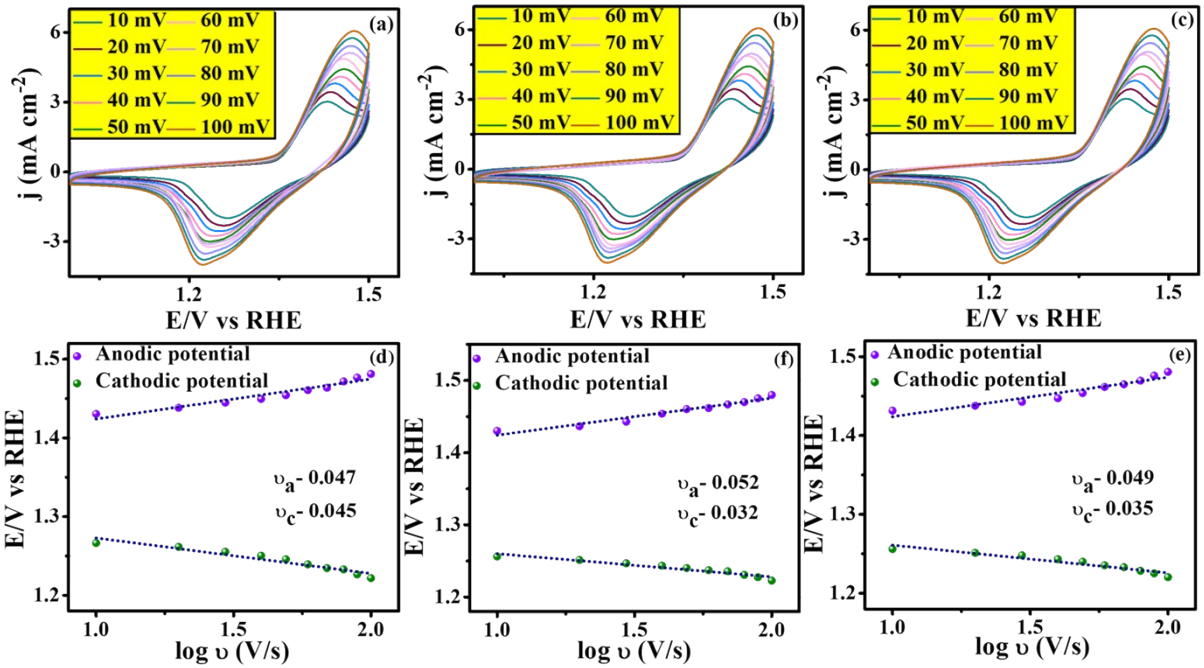

Figure S7. Cyclic voltammogram of Mo_2N at various pH of 14 (a), 13 (b) and 12 (c) with potential range of 10-100 mV and Peak potential of Mo_2N with respect to logarithm of scan rate [V/s] during CVs at various pH of 14 (d), 13 (e) and 12 (f) (Violet: anodic Peak; Green: cathodic peak)

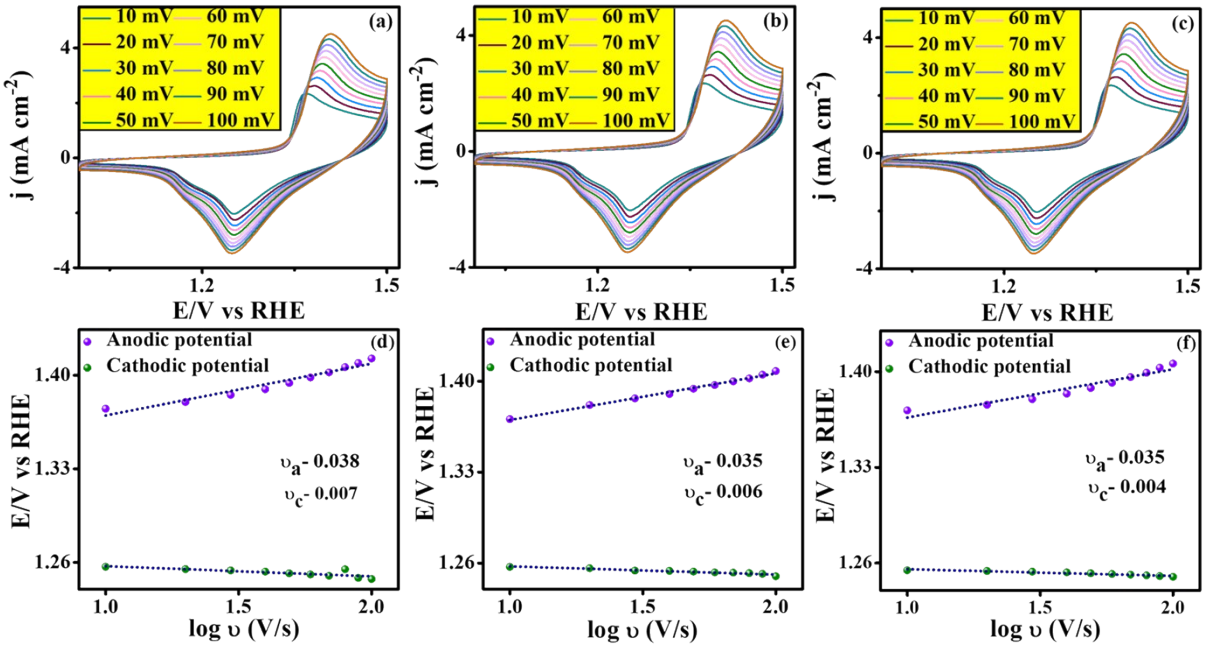

Figure S8. Cyclic voltammogram of CeF_3 at various pH of 14 (a), 13 (b) and 12 (c) with potential range of 10-100 mV and Peak potential of CeF_3 with respect to logarithm of scan rate [V/s] during CVs at various pH of 14 (d), 13 (e) and 12 (f) (Violet: anodic Peak; Green: cathodic peak)

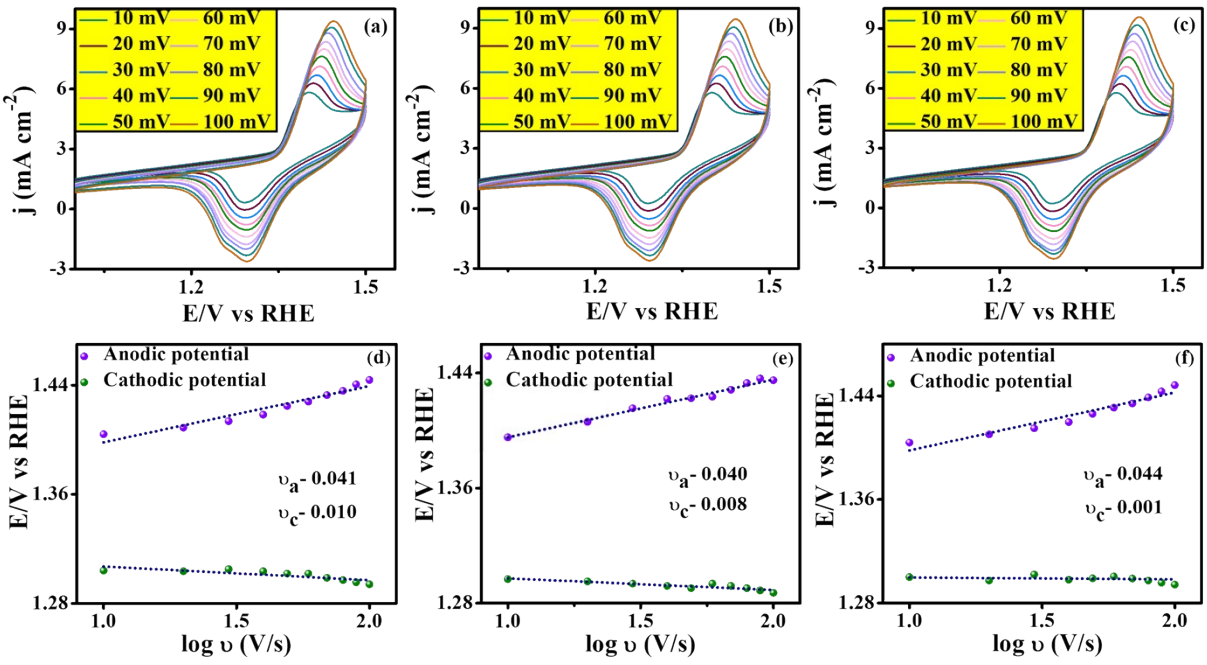

Figure S9. (a-c) Plots of redox peak current densities versus the square root of scan rates and (d-f) Laviron analysis of CeF_3@Mo_2N, Mo_2N and (f) CeF_3

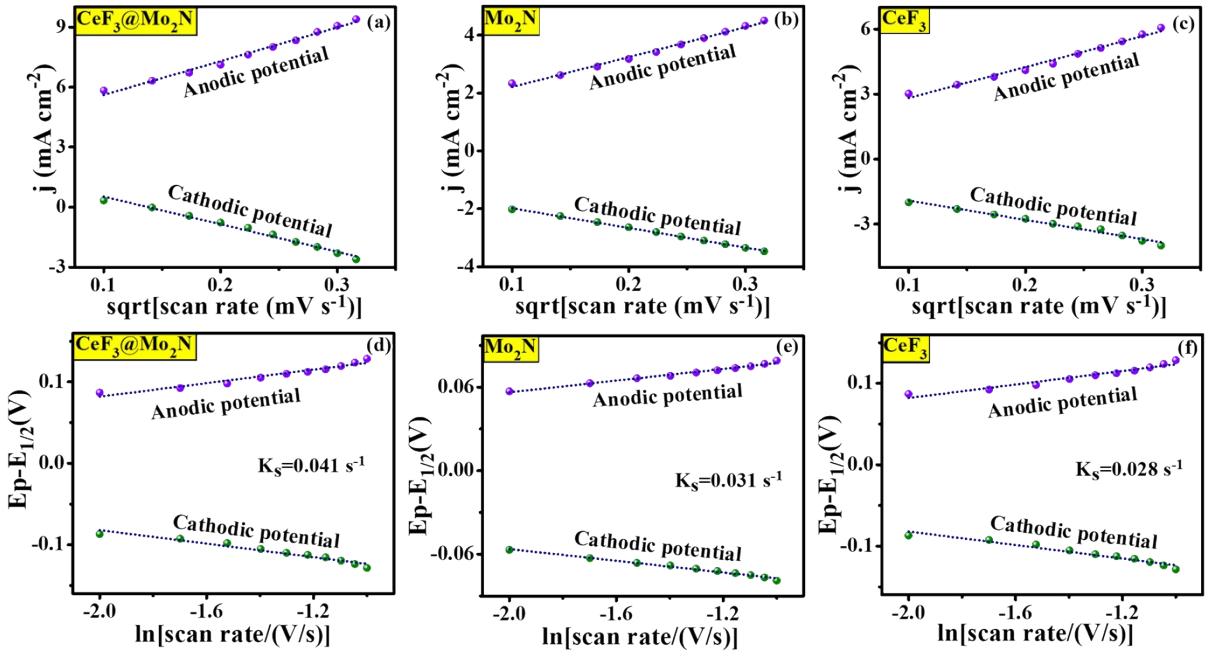

Figure S10. EGOR performance in alkaline water without iR-correction: (a) LSV polarization curves, (b) CV curve of CeF_3@Mo_2N, (c) Bar diagram of overpotential at various current density of CeF_3@Mo_2N, (d) Tafel plots derived from LSV curves, (e) Nyquist plot obtained from EIS at 1.59 V vs RHE (inset: Randles circuit) and (f) Chronopotentiometry curve of CeF_3@Mo_2N at current density of 10 mA cm^{-2}

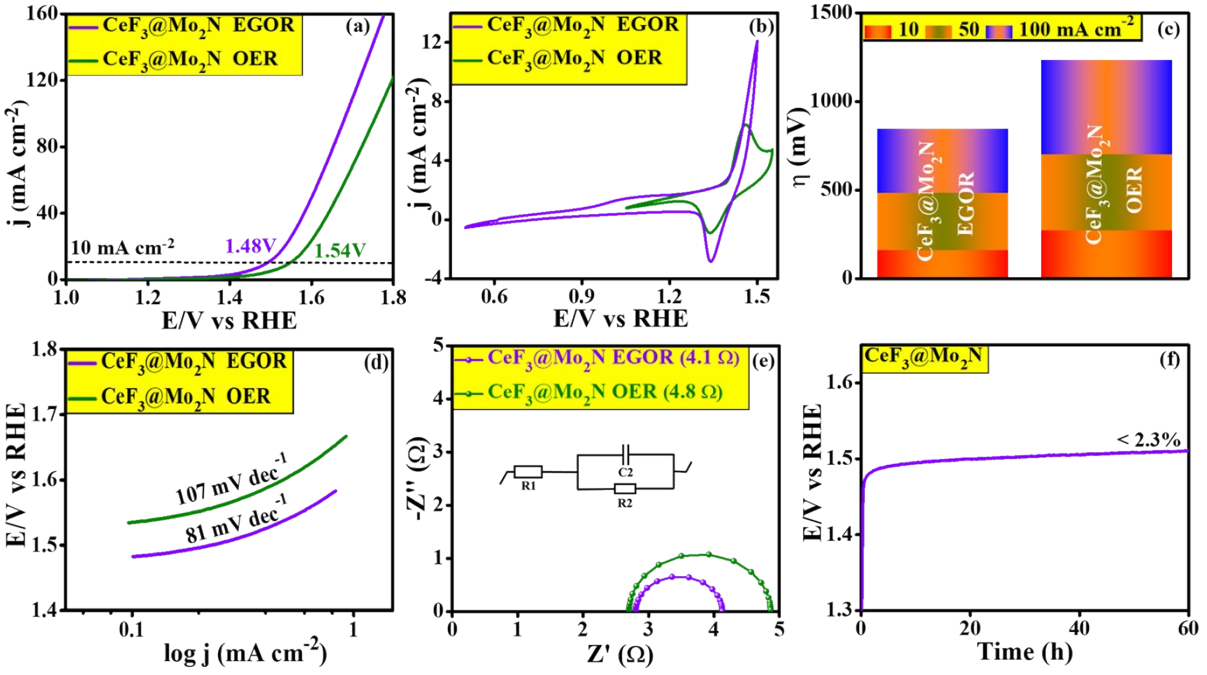

Figure S11. (a) ECSA-Normalized LSV curves, (b) Bet-Normalized LSV curves (c) Mass Normalized LSV curves (d) Mass activity of as prepared electrocatalysts, (e) Associated charges (AC) of CeF_3@Mo_2N, Mo_2N, CeF_3 and (f) TOF-Normalized LSV curves of HER

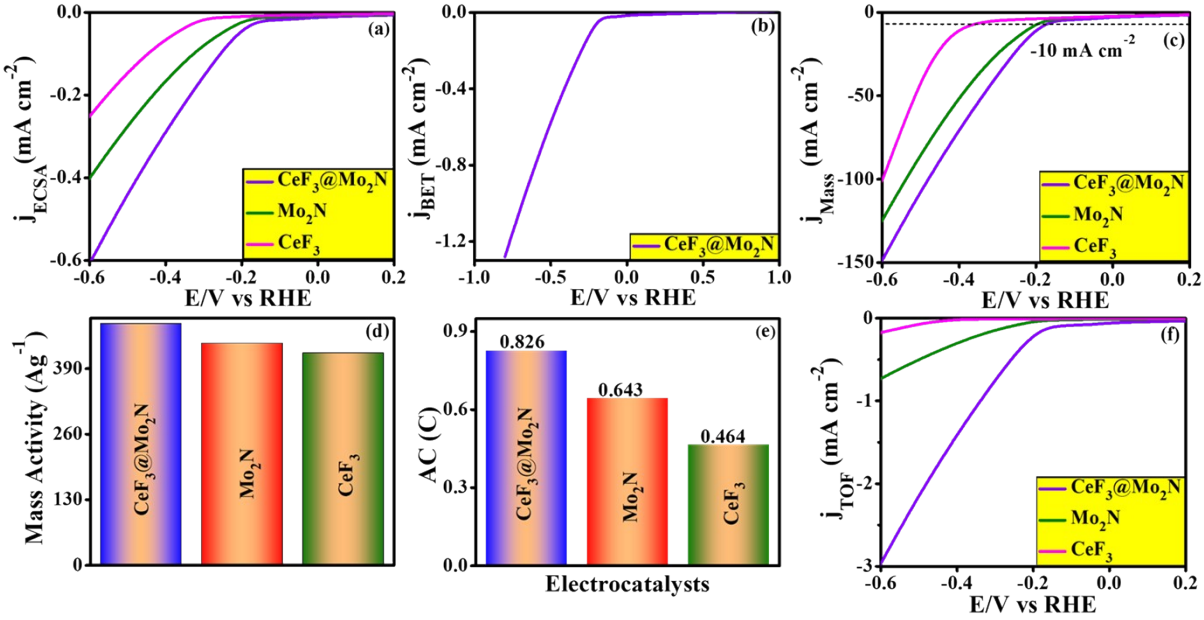

Figure S12. Bode plots at different potentials: (a) CeF_3@Mo_2N, (b) Mo_2N and (c) CeF_3, Nyquist plot measured at various applied voltages: (d) CeF_3@Mo_2N, (e) Mo_2N and (f) CeF_3

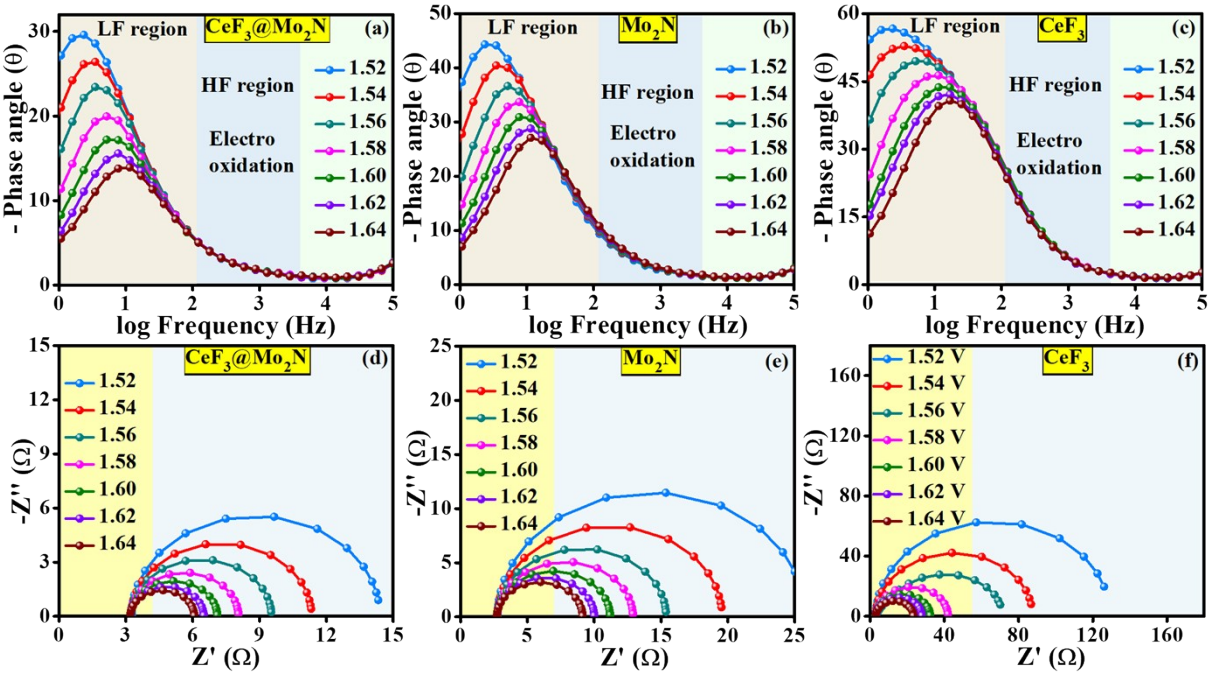

Figure S13. Mott-Schottky plots: (a,b) CeF_3 and Mo_2N; Tauc plots: (c,d) CeF_3 and Mo_2N and (e) Energy band diagram of CeF_3 and Mo_2N in CeF_3@Mo_2N under before and after Schottky contact

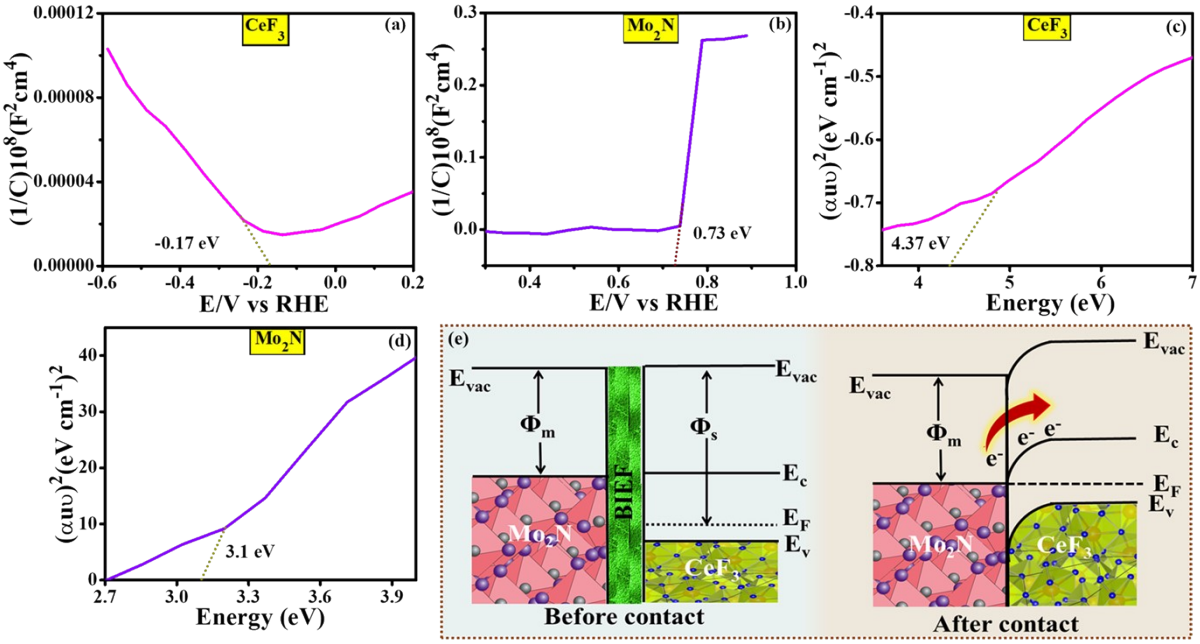

It is well known that band gap was determined from Tauc model by following the equation (hυ) as $(\alpha h\upsilon)^2 = A(h\upsilon - E_g)$, where α=2.303A/L (L-path length/10 mm, A-absorbance). The E_g of CeF_3 and Mo_2N was extracted by extrapolating the intercept of linear relation of $(\alpha h\upsilon)^2$ vs hυ to y=0.

Figure S14. Post –XPS spectra of CeF_3@Mo_2N: (a) Mo and (b) Ce

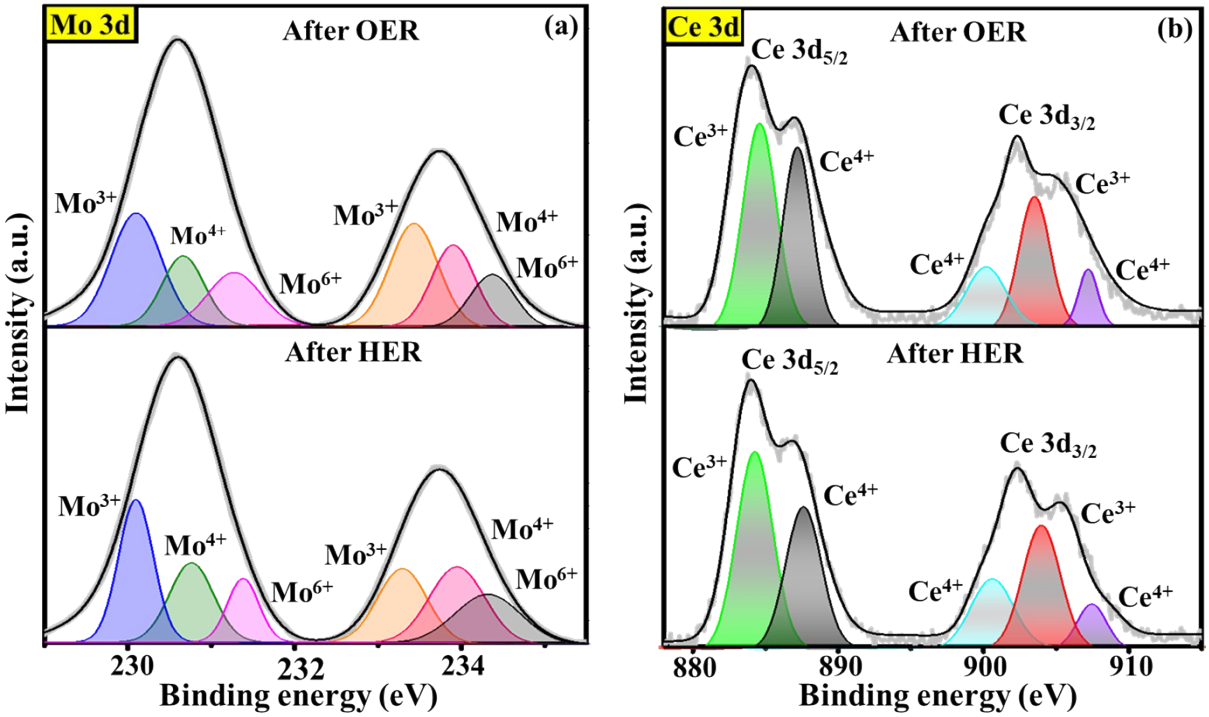

SI-IV. Tables

Table S1. Comparison of OER performance of CeF_3@Mo_2N with reported metal-based catalysts

S.No	Catalyst	Overpotential (mV)	Substrate	Reference
*	**CeF_3@Mo_2N**	**311**	**NF**	**Present work**
1	Ni_3N-CNTs	321	NF	S1
2	Ni_3N	370	NF	S2
3	Co_2N	390	NF	S3
4	Bulk Ni_3FeN	320	NF	S4
5	RuO_2/IF	348	NF	S5
6	Co_4N-CeF_3	320	GC	S6
7	Co-VN@C	330	NF	S7
8	$Ni_{0.42}Co_{0.58}F_2$-G	313	NF	S8
9	Co-Ni_3N	307	NF	S9
10	TiN@Ni_3N	350	CC	S10
11	Ni_3FeN	355	NF	S11
12	Ni_3N	325	GC	S12
13	Mo_2N	353	NF	S13
14	Co-Mo-N-PHP	325	CC	S14
15	WN/CC	325	NF	S15
16	$NiCo_2N$/NF	370	NF	S16
17	W_2N/WC	320	NF	S17
18	Co_3O_4-NC/N rGO	440	NF	S18
19	CoO-N-doped graphene	340	NF	S19
20	Co/VN	320	CC	S20
21	Co@NC-3/1	370	NF	S21
22	Co@Co_3O_4/NC	410	GC	S22
23	Ni_3N-Co_3N	320	NF	S23
24	Cu@CeO_2@NFC-0.25	340	GC	S24
25	CeOx/CoOx	350	NF	S25
26	CeO_2@PIZA/FTO	370	Au	S26
27	NCNTFs	370	NF	S27
28	PNC/Co	370	NF	S28
29	Co_3O_4@Z67-N700@CeO_2	351	NF	S29
30	Ce-NiO-E	382	CC	S30

Table S2: Collection Efficiency (N) value for the redox reaction of ferro-ferri in 0.1 M KNO_3 with 10 mM of $K_3[Fe(CN)_6]$ at various rotation speed by RRD electrode

S.No	Rotation speed (RPM)	Disc current (mA)	Ring current (mA)	Collection Efficiency (N)
1	300	0.36325	0.1031114	0.24053333
2	600	0.30500	0.0543410	0.17816393
3	900	0.43106	0.0777699	0.18025100
4	1200	0.67308	0.0687140	0.10208890
5	1500	0.37887	0.1376220	0.20117718

Table S3. Trumpet plot parameters: [(a)]Slope of the anodic peak; [(b)]Slope of the cathodic peak; [(c)]Electron transfer coefficient and [(d)]Standard rate constant of CeF_3@Mo_2N, Mo_2N and CeF_3

Catalysts	pH	v_a[V/log(V/s)][(a)]	v_c[V/log(V/s)][(b)]	α[(c)]	k^0 [1/s][(d)]
CeF_3@Mo_2N	12	0.0520	0.0323	0.6190	0.7657
	13	0.0491	0.0351	0.5833	0.8017
	14	0.0474	0.0452	0.5108	0.9223
Mo_2N	12	0.0353	0.0049	0.8781	0.0799
	13	0.0359	0.0063	0.8387	0.2087
	14	0.0387	0.0076	0.8358	0.2473
CeF_3	12	0.0447	0.0014	0.9696	0.0023
	13	0.0402	0.0081	0.8322	0.0528
	14	0.0412	0.0100	0.8046	0.2133

Table S4. Comparison of HER performance of CeF_3@Mo_2N with reported metal-based catalysts

S.No	Catalyst	Overpotential (mV)	Substrate	Reference
*	**CeF_3@Mo_2N**	**195**	**NF**	**Present work**
1	Ni_3Fe nitride	209	NF	S31
2	WN/rGO	265	NF	S32
3	Ni_3N	208	NF	S33
4	WS_2- NCNT	225	CC	S34
5	δ-WN/Fe	209	NF	S35
6	NiMoNx/C	220	GC	S36
7	$Co_{0.6}Mo_{1.4}N_2$	200	NF	S37
8	Fe-WCN	220	NF	S38
9	$Co_{0.75}Fe_{0.25}$@NC	202	NF	S39
10	Ni_3N nanosheets	350	CC	S40
11	Co_3O_4 NW	320	CC	S41
12	Co/VN/NC-1	250	GC	S42
13	Mo_2N/NC-2	217	NF	S43
14	Co-NRCNTs	260	NF	S44
15	Co@N-CNTs	275	NF	S45
16	Co-embedded N-CNTs	370	CC	S46
17	CoFe@NCNT	270	GC	S47
18	g-C_3N_4/N-doped graphene	240	NF	S48
19	g-C_3N_4 nanoribbon/graphene	207	NF	S49
20	U-CNT-900	270	NF	S50
21	C_3N_4@NG	240	NF	S51
22	g-C_3N_4/CeO_2/Fe_3O_4	310	NF	S52
23	3D–rGO–CeO_2	340	NF	S53
24	Mo_2C/CeO_2	220	NF	S54
25	CeO_2–Y_2O_3–Nd_2O_3	303	NF	S55
26	CeO_2/$Co(OH)_2$	317	NF	S56
27	Fe_xNi_y/CeO_2	240	NF	S57
28	1:1 CeO_2/CuO	245	NF	S58
29	CeO_2-NiCoP	242	NF	S59
30	CeO_2/Ni/NC	320	NF	S60

Table S5. Comparison of overall performance of CeF_3@Mo_2N with reported metal-based catalysts

S.No	Catalyst	Voltage (η_{10})	Reference
*	**CeF_3@Mo_2N**	**1.59**	**Present work**
1	Co-SCN-3/RGO	1.63	S61
2	Fe_2Ni_2N/NF	1.65	S62
3	$FeNi_3N$	1.62	S63
4	MoN-Co_2N/CP	1.63	S64
5	W_2N_3-10/Fe_2N	1.68	S65
6	Cu_3N	1.60	S66
7	NC@Cu_2CoxN	1.62	S67
8	Ni–Mo nitride	1.60	S68
9	Co-Mo_2C@NCNT	1.62	S69
10	Ni-N/CFC	1.62	S70
11	V-$FeNi_3N$/Ni_3N	1.63	S71
12	Nb-Ni_3N/NF	1.61	S72
13	Ni/Ni_3CNCNT 650-2	1.65	S73
14	PO-Ni/Ni-N-CNFs	1.69	S74
15	NiFe HNSs	1.70	S75
16	$NiCo_2O_4$ NW	1.63	S76
17	CoNi(OH)x||NiNx	1.65	S77
18	NiMoN||CoN	1.63	S78
19	CoMnO@CN	1.62	S79
20	S,N-Fe/N/C-CNT	1.60	S80
21	NC@CuCoNx	1.62	S81
22	CoN@VON	1.64	S82
23	$Co_{5.47}N$@NC	1.62	S83
24	Cu_1Ni_2N	1.63	S84
25	$FeNi_3N$/rGO	1.60	S85
26	Ce-doped CoP	1.65	S86
27	CeO_2-CuCoO/NF	1.63	S87
28	CoCe-Ni_3S_2/NF	1.68	S88
29	CeO_x/CoP/NF	1.63	S89
30	Fe_xNi_y/CeO_2/NC	1.70	S90

References

S1 T. Liu, M. Li, C. Jiao, M. Hassan, X. Bo, M. Zhou and H. L. Wang, *J. Mater. Chem. A*, 2017, **5**, 9377-9390.

S2 M. Shalom, D. Ressnig, X. Yang, G. Clavel, T. P. Fellinger and M. Antonietti, *J. Mater. Chem. A*, **2015**, ***3***, 8171-8177.

S3 P. Chen, K. Xu, Y. Tong, X. Li, S. Tao, Z. Fang, W. Chu, X. Wu and C. Wu, *Inorg. Chem. Front.*, **2016**, ***3***, 236-242.

S4 X. Jia, Y. Zhao, G. Chen, L. Shang, R. Shi, X. Kang, G. I. N. Waterhouse, L. Z. Wu, C. H. Tung and T. Zhang, *Adv. Energy Mater.*, **2016**, ***6***, 1502585-1502591.

S5 Y. Wu, Y. Liu, B. Liu, W. Jiang, T. Zhou, H. Li, M. Shang, J. Lang, C. Liu and G. Che, *ACS Appl. Nano Mater.*, **2022**, ***5***, 7714-7722.

S6 V. Pundir, A. Gaur, R. Kaur, Aashi and V. Bagchi, *ACS Sustainable Chem. Eng.*, **2025**, ***13***, 3491-3499.

S7 T. Peng, Y. Guo, Y. Zhang, Y. Wang, D. Zhang, Y. Yang, Y. Lu, X. Liu, P. K. Chu and Y. Luo, *Appl. Surf. Sci.*, **2021**, ***536***, 147982-147997.

S8 Z. Xu, W. Zuo, Y. Yu, J. Liu, G. Cheng and P. Zhao, *Adv. Sci.*, **2024**, ***11***, 2306758-2306768.

S9 C. Zhu, A. L. Wang, W. Xiao, D. Chao, X. Zhang, N. H. Tiep, S. Chen, J. Kang, X. Wang, J. Ding and J. Wang, *Adv. Mater.*, **2018**, ***30***, 1705516-1705533.

S10 Q. Zhang, Y. Wang, Y. Wang, A. M. Al-Enizi, A. A. Elzatahry and G. Zheng, *J. Mater. Chem. A*, **2016**, ***4,*** 5713-5718.

S11 G. Fu, Z. Cui, Y. Chen, L. Xu, Y. Tang and J. B. Goodenough, *Nano Energy*, **2017**, ***39***, 77-85.

S12 B. Ouyang, Y. Zhang, Z. Zhang, H. J. Fan and R. S. Rawat, *Small*, **2017**, ***13***, 1604265-1604275.

S13 L. Ma, L. R. L. Ting, V. Molinari, C. Giordano and B. S. Yeo, *J. Mater. Chem. A*, **2015**, ***3***, 8361-8368.

S14 H. Chu, D. Zhang, B. Jin and M. Yang, *Appl. Catal. B Environ.*, **2019**, ***255***, 117744-117770.

S15 J. Shi, Z. Pu, Q. Liu, A. M. Asiri, J. Hu and X. Sun, *Electrochim. Acta.*, 2015, **154**, 345-351.

S16 Y. Wang, B. Zhang, W. Pan, H. Ma and J. Zhang, *ChemSusChem.*, 2017, **10**, 4170-4177.

S17 J. Diao, Y. Qiu, S. Liu, W. Wang, K. Chen, H. Li, W. Yuan, Y. Qu and X. Guo, *Adv. Mater.*, 2020, **32**, 1905679-1905712.

S18 X. Han, G. He, Y. He, J. Zhang, X. Zheng, L. Li, C. Zhong, W. Hu, Y. Deng and T. Ma, *Adv. Energy Mater.*, 2018, **8**, 1702222-1702255.

S19 X. J. Cui, P. J. Ren, D. H. Deng, J. Deng and X. H. Bao, *Energy Environ. Sci.*, 2016, **9**, 123-129.

S20 X. Peng, C. Huang, J. Dai and Y. Liu, *Int. J. Hydrogen Energy*, 2022, **47**, 4386-4393.

S21 Y. Li, B. Jia, Y. Fan, K. Zhu, G. Li and C. Y. Su, *Adv. Energy Mater.*, 2018, **8**, 1702048-1702075.

S22 A. Aijaz, J. Masa, C. Rösler, W. Xia, P. Weide, A. J. Botz, R. A. Fischer, W. Schuhmann and M. Muhler, *Angew. Chem. Int. Ed.*, 2016, **55**, 4087-4091.

S23 C. Huang, B. Zhang, Y. Wu, Q. Ruan, L. Liu, J. Su, Y. Tang, R. Liu and P. K. Chu, *Appl. Catal. B Environ.*, 2021, **297**, 120461-120504.

S24 J. Xia, H. Zhao, B. Huang, L. Xu, M. Luo, J. Wang, F. Luo, Y. Du and C. H. Yan, *Adv. Funct. Mater.*, 2020, **30**, 1908367-1908389.

S25 J. H. Kim, K. Shin, K. Kawashima, D. H. Youn, J. Lin, T. E. Hong, Y. Liu, B. R. Wygant, J. Wang, G. Henkelman and C. B. Mullins, *ACS Catal.,* 2018, **8**, 4257-4265.

S26 D. J. Li, Z. G. Gu, W. Zhang, Y. Kang and J. Zhang, *J. Mater. Chem. A*, 2017, **5**, 20126-20130.

S27 B. Y. Xia, Y. Yan, N. Li, H. B. Wu, X. W. D. Lou and X. Wang, *Nat. Energy*, 2016, **1**, 1-8.

S28 X. Li, Z. Niu, J. Jiang and L. Ai, *J. Mater. Chem. A*, 2016, **4**, 3204-3209.

S29 X. Li, S. You, J. Du, Y. Dai, H. Chen, Z. Cai, N. Ren and J. Zou, *J. Mater. Chem. A*, 2019, **7**, 25853-25864.

S30 W. Gao, Z. Xia, F. Cao, J. C. Ho, Z. Jiang and Y. Qu, *Adv. Funct. Mater*., 2018, **28**, 1706056-1706064.

S31 H. P. Guo, B. Y. Ruan, W. B. Luo, J. Deng, J. Z. Wang, H. K. Liu and S. X. Dou, *ACS Catal*., 2018, **8**, 9686-9696.

S32 H. Yan, C. Tian, L. Wang, A. Wu, M. Meng, L. Zhao and H. Fu, *Angew. Chem. Int. Ed*., 2015, **54**, 6423-6427.

S33 Y. Zhang, B. Ouyang, J. Xu, S. Chen, R. S. Rawat and H. J. Fan*, Adv. Energy Mater.,* 2016, **6**, 1600221-1600227.

S34 Z. Wang, K. Zhao, H. Li, Z. Liu, Z. Shi, J. Lu, K. Suenaga, S. K. Joung, T. Okazaki, Z. Jin and Z. Gu, *J. Mater. Chem*., 2011, **21**, 171-180.

S35 H. Jin, H. Zhang, J. Chen, S. Mao, Z. Jiang and Y. Wang, *J. Mater. Chem. A*, 2018, **6**, 10967-10975.

S36 W. F. Chen, K. Sasaki, C. Ma, A. I. Frenkel, N. Marinkovic, J. T. Muckerman, Y. Zhu and R. R. Adzic, *Angew. Chem. Int. Ed.,* 2012, **51**, 6131-6135.

S37 B. Cao, G. M. Veith, J. C. Neuefeind, R. R. Adzic and P. G. Khalifah, *J. Am. Chem. Soc*., 2013, **135**, 19186-19192.

S38 Y. Zhao, K. Kamiya, K. Hashimoto and S. Nakanishi, *Angew. Chem*., 2013, **125**, 13883-13886.

S39 X. Zhao, P. Pachfule, S. Li, J. R. J. Simke, J. Schmidt and A. Thomas, *Angew. Chem*., 2018, **130**, 9059-9064.

S40 K. Xu, P. Chen, X. Li, Y. Tong, H. Ding, X. Wu, W. Chu, Z. Peng, C. Wu and Y. Xie, *J. Am. Chem. Soc*., 2015, **137**, 4119-4125.

S41 P. Chen, K. Xu, Z. Fang, Y. Tong, J. Wu, X. Lu, X. Peng, H. Ding, C. Wu and Y. Xie, *Angew. Chem*., 2015, **127**, 14923-14927.

S42 X. Li, Y. Huang, D. Chu, K. Kajiyoshi, Y. Liu, Y. Zhao, Q. Chen, R. Liu, L. Cao, L. Feng and J. Huang, *ACS Appl. Nano Mater*., 2025, **8**, 7026-7038.

S43 Y. J. Song and Z. Y. Yuan, *Electrochim. Acta.*, 2017, **246**, 536-543.

S44 X. Zou, X. Huang, A. Goswami, R. Silva, B. R. Sathe, E. Mikmeková and T. Asefa, *Angew. Chem*., 2014, **126**, 4461-4465.

S45 T. Ouyang, Y. Q. Ye, C. Y. Wu, K. Xiao and Z. Q. Liu, *Angew. Chem. Int. Ed*., 2019, **58**, 4923-4928.

S46 H. Vrubel and X. Hu, *Angew. Chem. Int. Ed.*, 2012, **51**, 12703-12706.

S47 J. Deng, P. Ren, D. Deng, L. Yu, F. Yang and X. Bao, *Energy Environ. Sci*., 2014, **7**, 1919-1923.

S48 Y. Zheng, Y. Jiao, Y. Zhu, L. H. Li, Y. Han, Y. Chen, A. Du, M. Jaroniec and S. Z. Qiao, *Nat. Commun*., 2014, **5**, 3783-3791.

S49 Y. Zhao, F. Zhao, X. Wang, C. Xu, Z. Zhang, G. Shi and L. Qu, *Angew. Chem. Int. Ed*., 2014, **53**, 13934-13939.

S50 S. Gao, G. D. Li, Y. Liu, H. Chen, L. L. Feng, Y. Wang, M. Yang, D. Wang, S. Wang and X. Zou, *Nanoscale*, 2015, **7**, 2306-2316.

S51 A. B. Laursen, S. Kegnæs, S. Dahl and I. Chorkendorff, *Energy Environ. Sci*., 2012, **5**, 5577-5591.

S52 J. Rashid, N. Parveen, T. u. Haq, A. Iqbal, S. H. Talib, S. U. Awan, N. Hussain and M. Zaheer, *ChemCatChem.*, 2018, **10**, 5587-5592.

S53 M. M. Liu, Z. Y. Ji, X. P. Shen, H. Zhou, J. Zhu, X. L. Xie, C. S. Song, L. R. Miao, X. L. Kong and G. X. Zhu, *Eur. J. Inorg. Chem*., 2018, **35**, 3952-3959.

S54 L. Tian, H. Liu, X. Yi, X. Wang, L. Pang and J. Li, *Int. J. Hydrogen Energy*, 2023, **48**, 23831-23841.

S55 T. Munawar, A. Bashir, K. M. Batoo, F. Mukhtar, M. S. Nadeem, S. Hussain, S. Manzoor, M. N. Ashiq, S. A. Khan, M. Koc and F. Iqbal, *J. Korean Ceram. Soc.,* 2024, **61**, 693-712.

S56 M. C. Sung, G. H. Lee and D. W. Kim, *J. Alloys Compd*., 2019, **800**, 450-455.

S57 L. Chen, H. Jang, M. G. Kim, Q. Qin, X. Liu and J. Cho, *Inorg. Chem. Front*., 2020, **7,** 470-476.

S58 D. Ghosh and D. Pradhan, *Langmuir*, 2023, **39**, 3358-3370.

S59 X. Guo, M. Li, L. Qiu, F. Tian, L. He, S. Geng, Y. Liu, Y. Song, W. Yang and Y. Yu, *Chem. Eng. J,* 2023, **453**, 139796-139805.

S60 L. Tian, H. Liu, B. Zhang, Y. Liu, S. Lv, L. Pang and J. Li, *ACS Appl. Nano Mater.*, 2021, **5**, 1252-1262.

S61 W. K. Jo, S. Moru and S. Tonda, *ACS Sustainable Chem. Eng*., 2019, **7**, 15373-15384.

S62 M. Jiang, Y. Li, Z. Lu, X. Sun and X. Duan, *Inorg. Chem. Front*., 2016, **3**, 630-634.

S63 B. Zhang, C. Xiao, S. Xie, J. Liang, X. Chen and Y. Tang, *Chem. Mater*., 2016, **28**, 6934-6941.

S64 W. Huang, Y. Tong, D. Feng, Z. Guo, R. Ye and P. Chen, *ChemSusChem.*, 2023, **16**, 202202078-202202085.

S65 T. Kavinkumar, H. Yang, A. T. Sivagurunathan, H. Jeong, J. W. Han and D. H. Kim, *Small*, 2023, **19**, 2300963-2300971.

S66 C. Panda, P. W. Menezes, M. Zheng, S. Orthmann and M. Driess, *ACS Energy Lett*., 2019, **4**, 747-754.

S67 J. Zheng, X. Chen, X. Zhong, S. Li, T. Liu, G. Zhuang, X. Li, S. Deng, D. Mei and J. G. Wang, *Adv. Funct. Mater*., 2017, **27**, 1704169-1704180.

S68 Z. Yin, Y. Sun, C. Zhu, C. Li, X. Zhang and Y. Chen, *J. Mater. Chem. A*, 2017, **5**, 13648-13658.

S69 L. Ai, J. Su, M. Wang and J. Jiang, *ACS Sustainable Chem. Eng*., 2018, **6**, 9912-9920.

S70 F. Yan, Y. Wang, K. Li, C. Zhu, P. Gao, C. Li, X. Zhang and Y. Chen, *Chem. Eur. J,* 2017, **23**, 10187-10194.

S71 J. Wang, Y. Sun, Y. Qi and C. Wang, *ACS Appl. Mater. Interfaces*, 2021, **13**, 57392-57402.

S72 J. Xiang, W. Zou and H. Tang, *Catal. Sci. Technol*., 2021, **11**, 6455-6461.

S73 T. Dong, X. Zhang, Y. Cao, H. S. Chen and P. Yang, *Inorg. Chem. Front*., 2019, **6**, 1073-1080.

S74 Z. Y. Wu, W. B. Ji, B. C. Hu, H. W. Liang, X. X. Xu, Z. L. Yu, B. Y. Li and S. H. Yu, *Nano Energy*, 2018, 51, 286-293.

S75 X. Sun, Q. Shao, Y. Pi, J. Guo and X. Huang, *J. Mater. Chem. A*, 2017, **5**, 7769-7775.

S76 A. Sivanantham, P. Ganesan and S. Shanmugam, *Adv. Funct. Mater*., 2016, **26**, 4661-4672.

S77 S. Li, Y. Wang, S. Peng, L. Zhang, A. M. Al-Enizi, H. Zhang, X. Sun and G. Zheng, *Adv. Energy Mater*., 2016, **6**, 1501661-1501668.

S78 Y. Zhang, B. Ouyang, J. Xu, G. Jia, S. Chen, R. S. Rawat and H. J. Fan, *Angew. Chem.,* 2016, **128**, 8812-8816.

S79 Y. P. Zhu, Y. P. Liu, T. Z. Ren and Z. Y. Yuan, *Adv. Funct. Mater.,* 2015, **25**, 7337-7347.

S80 P. Chen, T. Zhou, L. Xing, K. Xu, Y. Tong, H. Xie, L. Zhang, W. Yan, W. Chu, C. Wu and Y. Xie, *Angew. Chem.*, 2017, **129**, 625-629.

S81 J. Li, X. Kong, M. Jiang and X. Lei, *Inorg. Chem. Front*., 2018, **5**, 2906-2913.

S82 S. Dutta, A. Indra, Y. Feng, H. Han and T. Song, *Appl. Catal. B Environ*., 2019, **241**, 521-527.

S83 Z. Chen, Y. Ha, Y. Liu, H. Wang, H. Yang, H. Xu, Y. Li and R. Wu, *ACS Appl. Mater. Interfaces*, 2018, **10**, 7134-7144.

S84 Z. Wang, L. Xu, F. Huang, L. Qu, J. Li, K. A. Owusu, Z. Liu, Z. Lin, B. Xiang, X. Liu and K. Zhao, *Adv. Energy Mater.,* 2019, **9**, 1900390-1900401.

S85 Y. Gu, S. Chen, J. Ren, Y. A. Jia, C. Chen, S. Komarneni, D. Yang and X. Yao, *ACS Nano.,* 2018, **12**, 245-253.

S86 J. Li, S. Zou, X. Liu, Y. Lu and D. Dong, *ACS Sustainable Chem. Eng*., 2020, **8**, 10009-10016.

S87 L. Li, L. Cao, Q. He, B. Shang, J. Chen, J. Lei, N. Li and F. Pan, S*ustain. Energy Fuels*, 2020, **4**, 2775-2781.

S88 Z. Yu, S. N. Song, Y. W. Dong, X. T. Gao, Q. F. Jiang and Z. Zhao, *ACS Appl. Nano Mater*., 2024, **8**, 894-903.

S89 T. Zhang, X. Wu, Y. Fan, C. Shan, B. Wang, H. Xu and Y. Tang, *ChemNanoMat.,* 2020, **6**, 1119-1126.

S90 L. Chen, H. Jang, M. G. Kim, Q. Qin, X. Liu and J. Cho, *Inorg. Chem. Front*., 2020, **7**, 470-476.